Clinical Evaluation of Processing Techniques for Attenuation Correction with ^{137}Cs in Whole-Body PET Imaging

François Bénard, Robin J. Smith, Roland Hustinx, Joel S. Karp and Abass Alavi

Department of Radiology, University of Pennsylvania, Philadelphia, Pennsylvania

Transmission scanning can be successfully performed with a ^{137}Cs single-photon emitting point source for three-dimensional PET imaging. However, the attenuation coefficients provided by this method are underestimated because of the energy difference between 662- and 511-keV photons, as well as scatter and emission contamination when the transmission data are acquired after injection. The purpose of this study was to evaluate, from a clinical perspective, the relative benefits of various processing schemes to resolve these issues. **Methods:** Thirty-eight whole-body PET studies acquired with postinjection singles transmission scans were analyzed. The transmission images were processed and applied to the emission data for attenuation correction. Three processing techniques were compared: simple segmentation (SEG) of the transmission scan, emission contamination subtraction with scaling (ECS) of the resulting data to 511-keV attenuation coefficient values and a hybrid technique performing partial segmentation of some tissue densities on the ECS scan (THR). The corrected emission scans were blindly assessed for image noise, the presence of edge artifacts at the lung–soft-tissue interface and for overall diagnostic confidence using a semiquantitative scoring system. The count densities and the SDs in uniform structures were compared among the various techniques. The observations for each method were compared using a paired *t* test. **Results:** The SEG technique produced images that were visually less noisy than the ECS method ($P < 0.0001$) and the THR technique, but at the expense of increased edge artifacts at the boundaries between the lungs and surrounding tissues. The THR technique failed to eliminate these artifacts compared with the ECS technique ($P < 0.0001$) but preserved the activity gradients in the hilar areas. The count densities (and thus, the standardized uptake values) were similar among the three techniques, but the SEG method tended to underestimate the activity in the lung fields and in chest tumors (slope = 0.79 and 0.94, respectively). **Conclusion:** For many clinical applications, SEG data remain an efficient method for processing ^{137}Cs transmission scans. The ECS method produced noisier images than the other two techniques but did not introduce artifacts at the lung boundaries. The THR technique, more versatile in complex anatomic areas, allowed good preservation of density gradients in the lungs.

Key Words: attenuation correction; segmentation; PET

J Nucl Med 1999; 40:1257–1263

Received Aug. 28, 1998; revision accepted Feb. 4, 1999.

For correspondence or reprints contact: Abass Alavi, MD, Division of Nuclear Medicine, Hospital of the University of Pennsylvania, 3400 Spruce St., Donner Bldg. 110, Philadelphia, PA 19130.

The use of [^{18}F]fluorodeoxyglucose (FDG) PET scanning in cancer imaging has been growing rapidly in recent years (*1*). In clinical practice, the nuclear medicine physician is frequently faced with the dilemma of deciding whether measured attenuation correction is worthwhile to make an accurate diagnosis in every case (*2*). To improve the efficiency of clinical FDG PET imaging while maintaining quantitative accuracy, we implemented a technique to obtain rapid transmission images with a single-photon (^{137}Cs) point source in a sodium-iodide volume-imaging (three-dimensional) scanner (PENN PET 240H; UGM Medical Systems, Inc., Philadelphia, PA)(*3–5*). Because the position of the point source is known at all times, coincidence detection is not a requirement to localize the origin of the emitted photon: all detected singles events are assumed to come from the point source. The transmission scans obtained with this method do not provide identical attenuation coefficients to 511-keV photons, because the energy of the γ-rays of ^{137}Cs are higher (662 keV). Furthermore, despite the good energy resolution of sodium-iodide–based systems, some of the emission activity present in the field of view (FOV) during postinjection transmission scanning may spill into the energy window for the 662-keV photons. In addition, only energy windowing is available as a method to suppress scatter contamination of the transmission photon. The scatter contamination in the transmission data lowers measured attenuation coefficients. To overcome these limitations, we have used image segmentation (SEG) to assign 511-keV population-average attenuation coefficients in the lung and nonpulmonary soft-tissue areas of the transmission scan (*3*). The transmission image is then forward projected (converted to a sinogram by projecting the image data along the sampled angles). The resulting sinogram is used to correct the emission data for attenuation. This technique, which we have applied to hundreds of clinical patients, also has the advantage of eliminating the noise component of the transmission scan and improving the final image quality. However, this approach has several drawbacks.

First, the lung density can change in some pathologic states, and small pulmonary nodules may not be assigned the proper attenuation coefficient by the segmentation algo-

rithm. The hilar area, an important site of nodal metastases, has a variable density as the bronchial and vascular trees fan away from the mediastinum. In some areas, such as in the head and neck, additional densities can be encountered (e.g., bone structures, air passages). Simple segmentation algorithms will recognize only two densities within the body: lung and soft tissues. With more densities, clear rules to distinguish one tissue area from another become difficult to implement reliably. At the periphery of the lungs, notably the diaphragm and the lung apices, respiratory motion will average the density of attenuating tissues to an intermediate value between the lungs and soft-tissue equivalents. The segmentation algorithm, which must choose between only two values, may miscalculate the attenuation in these areas, enhancing the periphery of the lungs. Our particular implementation of the segmentation algorithm suffers from an additional limitation: the segmentation process fails when more than one body contour is encountered. This is problematic in some situations, such as when the arms are in the FOV or when scanning the lower extremities.

To overcome these limitations, we have implemented two alternative methods to process the ^{137}Cs transmission scans. One approach, emission contamination subtraction and scaling (ECS), measures the emission contamination present in the transmission scan, subtracts this measurement from the transmission data and scales the resulting image to 511-keV attenuation coefficients (*5*). The other approach is a hybrid technique combining the ECS method with partial image segmentation (THR) (*6,7*). The quantitative accuracy of these methods was assessed in phantom and preliminary clinical data against coincidence transmission data and was found to be within 5% of each other (*5*) and within 10% of coincidence transmission data (*3*). The later difference was largely the result of the presence of scatter in coincidence transmission scans, lowering the attenuation coefficients to 0.091 cm^{-1} in water (the expected value for 511-keV photons is 0.095 cm^{-1}). The purpose of this study was to evaluate, from a clinical perspective, the relative merits of each processing technique (SEG, ECS and THR) in routine whole-body PET scanning.

MATERIALS AND METHODS

Patient Population

Forty consecutive whole-body FDG PET studies from patients referred for cancer imaging were selected for this study. No special selection criteria were used, but each patient had to undergo an FDG PET study (usually neck to groin), followed by transmission scanning of the same area with a ^{137}Cs point source. No preference was given to weight, sex, age or disease status. Two cases were excluded from further consideration because the lungs were not in the FOV; 38 cases were available therefore for analysis. The acquisition of the study did not significantly differ from the normal clinical protocol, except for the additional measurement of a short 8-s emission contamination scan at each bed position.

Instrumentation

The studies were all acquired on a PENN-PET 240H scanner, a sodium-iodide–based system without interplane septa, that functions as a full-time volume-imaging scanner (*8*). The scanner, with a hexagonal arrangement of six large NaI(Tl) detectors (50 × 20 × 2.5 cm), has an axial FOV of 128 mm and a transverse FOV 512 mm in diameter. The spatial resolution at the center is 5.5 mm in all three planes. The system sensitivity is approximately 150 Kcps/μCi/mL.

Emission Scanning

All the clinical studies were performed after the intravenous injection of 4.218 MBq/kg FDG. Sixty to 90 min after the injection, the patient was positioned in the scanner, feet first, arms upraised and folded over the head. Several emission scans were then acquired at overlapping 6.4-cm intervals to ensure uniform sensitivity over the FOV. The scan duration at each bed position varied from 4 to 5 min. A typical whole-body scan comprised seven to nine bed positions to cover the area between the neck and the groin, for a total acquisition time varying between 35 and 55 min. The images were reconstructed with the ordered subsets expectation maximization, an iterative reconstruction algorithm that has been shown to be both practical and effective in obtaining high-quality images from emission and transmission data (*9,10*).

Transmission Scan Acquisition

A 22 MBq ^{137}Cs point source was mounted in a holder at a radius of 37 cm from the center of the transverse FOV, in the center of the axial FOV. This source was shielded from the near detector and rotated around the patient at a speed of 1 revolution per 54 s. The transmission scan was acquired with an energy window setting set at 625–800 keV to reduce contamination by 511-keV emission rays. Sequential transmission scans were acquired at several overlapping bed positions to cover the same area as the emission acquisition, after completion of the emission study. Successive transmission scans were displaced 5.6 cm axially to maintain a uniform sensitivity (*5*). More bed positions are used for transmission than for emission studies to compensate for the shorter FOV available with this method. The acquisition software keeps track of the exact bed positions to assemble the data precisely before applying the attenuation correction. After the transmission scan, the ^{137}Cs point source was removed, and a short (8-s) emission contamination (EC) scan was acquired without the source in the FOV to obtain an estimate of the counts as a result of the emission activity in the 625- to 800-keV energy window. This contamination results from spillover of photons from the activity present in the patient after an injection of [^{18}F]FDG. These photons overlap into the transmission scan energy window as a result of the finite energy resolution of the detectors. The EC scan was acquired with all the same settings as the transmission scan, the only difference being the absence of the transmission source in the FOV. A longer EC scan duration was not needed, because the measured EC distribution activity is relatively uniform and can be smoothed to a level that does not introduce additional noise.

Transmission Scan Processing

The transmission scan was divided by the blank scan, and the log of this ratio was reconstructed with the ordered subsets expectation maximization algorithm, using two iterations of eight subsets each. A Gaussian filter with an 8-mm full-width-at-half-maximum kernel was used to smooth the data between each iteration. The image was then segmented using values of 0.095 cm^{-1} for the nonpulmonary

soft tissues and 0.026 cm^{-1} for the lungs, forward projected and applied to the emission data before reconstruction (*3*).

Alternatively, the ECS method was applied to the transmission data (*5*). Briefly, the EC scan is first subtracted from the transmission scan. The ECS corrects the measured attenuation coefficients from 0.073 ± 0.002 cm^{-1} to 0.085 ± 0.003 cm^{-1} (for an expected 662-keV attenuation coefficient of 0.086 cm^{-1}). The resulting scan then reflects pure transmission data, but the attenuation coefficients are underestimated compared with 511-keV value as a result of both the higher energy photons and residual scatter. Simple linear scaling of the median soft-tissue attenuation values from 0.085 to 0.095 cm^{-1} provides a good estimate of the distribution of soft-tissue and lung densities, without segmentation. This 30% increase makes the attenuation coefficients obtained with this method quantitatively comparable with those of SEG and measured coincidence attenuation correction (*5*). The EC scan effectively reduces the variability of the measured (662 keV) transmission attenuation coefficient across studies and patients (*5*).

The THR approach is designed to combine the advantages of the SEG and ECS methods. Basically, a threshold is applied to the final EC scan to reduce the count variations in areas of uniform density. Pixels above a predefined density (0.078 cm^{-1}) are set to the known value for 511-keV attenuation coefficients in soft tissues (0.095 cm^{-1}). Pixels corresponding to lung attenuation coefficients (below a threshold of 0.048 cm^{-1}) are left unchanged to preserve density gradients across the lungs. Pixels of intermediate values (0.048–0.078 cm^{-1}) are linearly interpolated. This approach maintains pulmonary and hilar density gradients, while reducing the noise contribution from the water-equivalent soft-tissue areas. The attenuation coefficients of nonpulmonary tissues are consistent within and across individuals.

Data Analysis

To assess image quality, a subjective scoring system was used. Two observers assessed the presence of image noise, linear artifacts at the tissue boundaries and overall image quality. No observer training was performed before analyzing the studies; both readers were experienced in the interpretation of both attenuation-corrected and uncorrected clinical PET images. The overall perception of image noise and lesion detection confidence was scored from 0 (flawless image with no noise fluctuations) to 4 (noninterpretable image). The presence of linear artifacts at tissue boundaries such as the lung-mediastinal interface, the diaphragm, the lateral aspects of the lungs and the apices was scored from 0 (no linear area of increased uptake) to 4 (intensely increased uptake that could be confused with disease). The attenuation-corrected images were compared with uncorrected images to determine whether similar abnormalities were detected by both. The overall image quality was subjectively rated from 0 (excellent image quality) to 4 (noninterpretable study). The readers were blinded as to which processing method had been used to reconstruct the fully corrected image sets being assessed. A total of 234 qualitative interpretations were available for analysis (two readers × three processing methods × 38 studies). The processing methods (ECS, THR and SEG) were compared with each other using the Wilcoxon signed rank test. The Bonferroni correction for multiple comparisons was not applied, because differences among these datasets were hypothesized a priori.

Regions of interest (ROIs) were drawn in uniform structures such as the periphery of the lungs and the liver, excluding any area of visually increased focal uptake. No organ is purely uniform in the human body, but this approach was selected with the assumption that a lower relative pixel-to-pixel fluctuation in these ROIs reflects a lower noise content. The ROI size varied from 100 to 300 pixels for the lungs and 80–200 pixels for the liver, with a pixel volume of 0.064 mL (4 × 4 × 4 mm^3). Identical regions were applied to the three sets (SEG, ECS and THR) of images. Quantitatively, the pixel-to-pixel SDs reflect the noise in uniform structures. These measurements were compared using paired *t* tests for the uniform area (lungs and liver). Additional ROIs of an average size of 50 pixels were drawn over hypermetabolic lesions in the chest when present, or in the myocardium, to assess the quantitative reproducibility of the three methods. The Pearson correlation coefficients and the regression slopes were calculated to compare the quantitative accuracy of each method relative to each other.

RESULTS

Qualitative Analysis

The various steps involved in complete reconstruction of the transmission scans are illustrated in Figure 1. The uncorrected transmission images obtained with a ^{137}Cs point source were of outstanding quality (Fig. 1, top row), albeit with inaccurate attenuation coefficients. The ECS method maintained the overall image quality (Fig. 1, second row), while subtracting the emission contamination and scaling the attenuation coefficients for correct 511-keV values. As in the raw transmission scan, the density gradients were well preserved in the lungs, but the soft tissue still presented significant pixel-to-pixel variations as a result of statistical noise. The segmented transmission image (Fig. 1, third row) did not propagate noise and was scatter free. This was achieved at the expense of loss of density gradients, especially in the pulmonary parenchyma. The THR method (Fig. 1, fourth row), a compromise between the ECS and SEG methods, produced uniform attenuation coefficients over the nonpulmonary soft-tissue values, yet maintained the density gradients in the lung parenchyma.

The visual impact of these various processing techniques on the final reconstructed images was subtle. Figure 2 shows emission images (from the same study as the transmission images in Fig. 1) reconstructed with measured transmission scans from the various methods. The uncorrected image (Fig. 2, top row) is immediately recognizable by the presence of activity outside the patient, the high pulmonary activity and the enhanced body outlines. The ECS scan (Fig. 2, second row) is noisier, as a result of propagation of noise from the transmission scan in the reconstruction process. In this particular patient, SEG and THR produced almost identical images (Fig. 2, third and fourth rows) of excellent quality with less noise than the ECS images.

The results of qualitative interpretations of all the emission studies reconstructed with the various attenuation correction methods are shown in Table 1. In this table, a single value is reported for each method because the scores of the two readers were averaged to provide three sets (SEG, ECS and THR) of 38 studies. Analyzing the data of each reader separately yielded similar results for both. The ECS

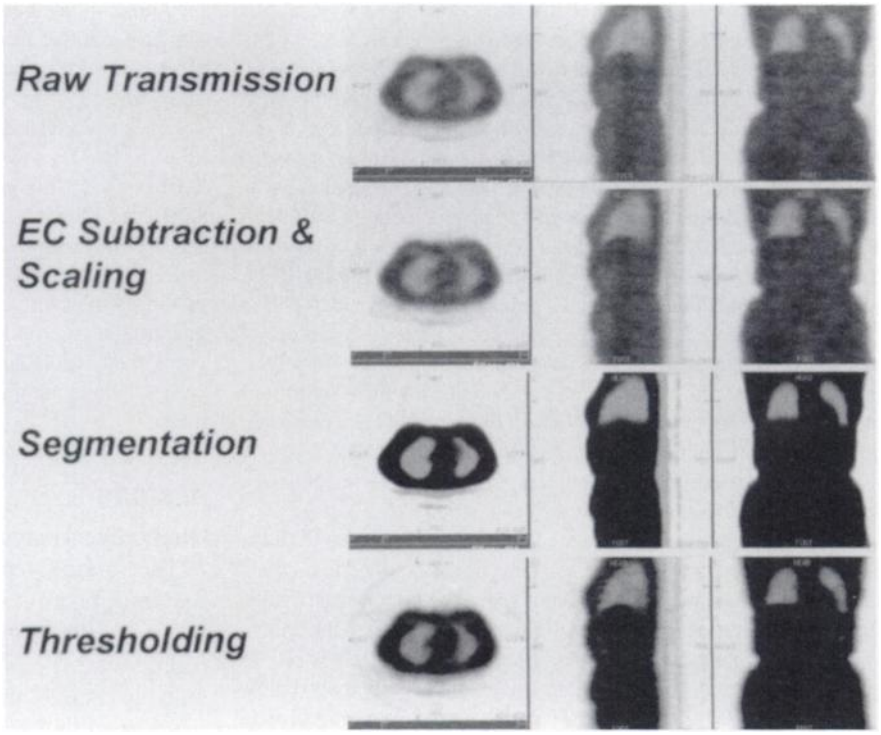

FIGURE 1. Transmission scans resulting from various processing methods. Top row shows uncorrected transmission image. Second row shows results from ECS method, which produces few apparent changes in transmission image quality but assigns accurate attenuation coefficients. Third and fourth rows show transmission images resulting from SEG and THR methods, respectively.

images were significantly noisier than those obtained with the SEG or THR methods. However, the ECS method introduced fewer perceptible edge artifacts at the lung–soft-tissue boundaries. Segmentation produced images that on overall appearance were more pleasing to physicians than the other methods, mainly because of reduced noise in the final images. Segmentation did introduce some artifacts that are well illustrated by the study in Figure 3. The top row shows the uncorrected emission data. The second row shows the fully reconstructed image using the ECS method, whereas the third and fourth rows show the results of the SEG and THR methods, respectively. As expected, the resulting image from the SEG method is of high quality, with a low noise content. However, on close examination, it

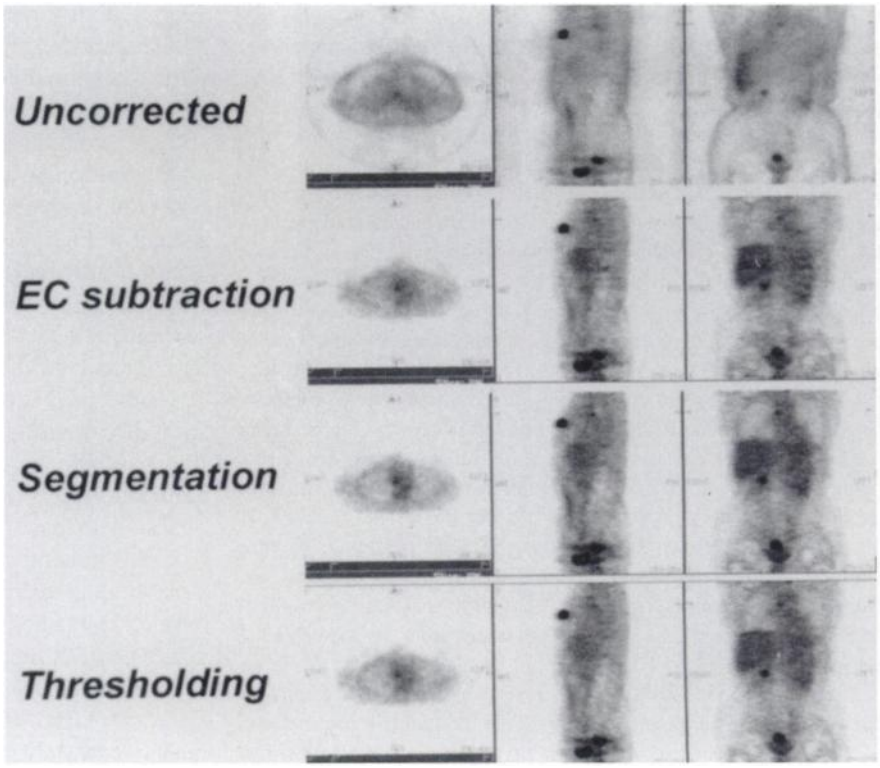

FIGURE 2. Corresponding emission images from same patient as in Figure 1. All processing methods produce images of good quality, but ECS images (second row) are slightly noisier. SEG and THR images (third and fourth rows, respectively) are virtually identical, except perhaps for minimal increase in activity at diaphragmatic boundary overlying liver in THR image (fourth row).

TABLE 1
Qualitative Analysis

	SEG	ECS	THR
Overall image quality (0–4)	0.86 ± 0.76	1.53 ± 1.11	1.08 ± 0.98
	← $P < 0.0001$ →	← $P < 0.0001$ →	
	← $P < 0.01$ →		
Edge artifacts (0–4)	0.36 ± 0.41	0.16 ± 0.27	0.41 ± 0.43
	← $P < 0.0001$ →	← $P < 0.0001$ →	
	← P = ns →		
Image noise (0–4)	1.11 ± 0.59	1.70 ± 0.79	1.33 ± 0.74
	← $P < 0.0001$ →	← $P < 0.0001$ →	
	← $P < 0.01$ →		

ns = not significant.

Summary of results of qualitative interpretation performed to identify perceived differences on final scans with three processing techniques (SEG = segmentation; ECS = emission contamination subtraction and scaling; THR = thresholding). Numbers represent qualitative scores (detailed in methods section) with SDs, where 0 represents flawless image. *P* values were calculated with Wilcoxon signed rank test. Systematic trends explain why small differences (such as with image noise scores) become highly significant.

becomes apparent that the activity in the hila and the apices of the lungs is underestimated, with loss of the normal activity gradient (Fig. 3, arrows). These gradients were always well preserved on the ECS and THR images. Because of the choice of thresholds used for the THR method, some edge artifacts were also visually perceptible along the lung outlines (Table 1 and Fig. 3, fourth row, at the surface of the diaphragm), because the software needs a cutoff to start segmenting the soft-tissue values.

Quantitative Analysis

The image noise was also quantitatively assessed by measuring the pixel-to-pixel variations at the periphery of the liver, an organ with a uniform activity distribution in the absence of disease on FDG PET images. Confirming the findings of qualitative evaluation, this analysis demonstrated significantly lower variations for the SEG and THR methods compared with the ECS method (Table 2). Although the THR method tended to produce slightly noisier images than with SEG, the difference did not reach statistical significance ($P = 0.099$).

The count density measurements from the fully corrected images were in good agreement among all methods, as illustrated in Figure 4. The SEG technique tended to underestimate the counts in the lung parenchyma compared with the ECS technique (Fig. 4B), with a regression slope of 0.79 ± 0.05 ($r = 0.92$). The count density measurements of active lesions in the chest (or part of the left ventricle, if no lesion could be identified on the scan) were in good agreement (slope = 0.94 ± 0.05; $r = 0.94$) with the SEG approach (Fig. 4A), with some exceptions. The activity in some small pulmonary nodules can be underestimated if the segmentation process does not segment appropriately the nodule on the transmission scan as a soft-tissue density. These phenomena do not occur with the THR technique, hence, a closer correlation between the THR and ECS methods for count density measurements ($r = 0.99$ and 0.98 for thoracic lesion and lung parenchyma counts, respectively, Figs. 4C and D).

DISCUSSION

PET has evolved progressively from a research tool to become a mainstream clinical procedure. Although the research use of PET requires quantitative precision and accuracy, good clinical operation requires rapid patient throughput, excellent image quality for interpretation purposes and excellent overall diagnostic accuracy. Some

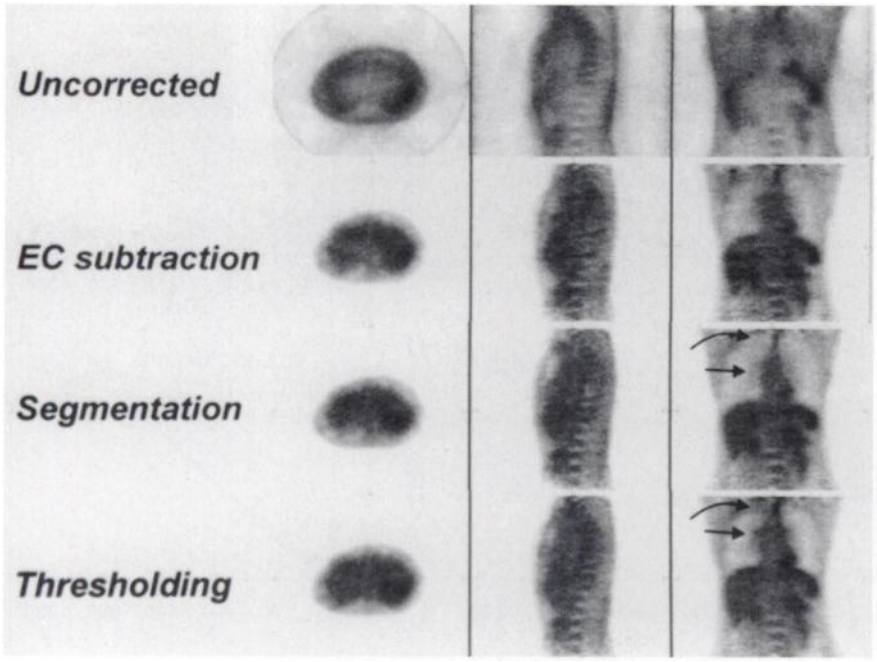

FIGURE 3. Emission images from another patient. Uncorrected images are shown in top row. In this case, SEG method (third row) subtly underestimated uptake in apices (curved arrows) and hila (straight arrows), compared with ECS and THR images (second and fourth rows, respectively).

TABLE 2
Quantitative Analysis for Image Noise

SEG	ECS	THR
0.210 ± 0.003	0.244 ± 0.005	0.220 ± 0.064
← $P < 0.001$ →	← $P < 0.001$ →	
← $P = 0.099$ →		

Quantitative analysis of image noise in final reconstructed image (SEG = segmentation; ECS = emission contamination subtraction and scaling; THR = thresholding). Noise was measured by drawing curvilinear region of interest at periphery of liver, in area devoid of visually identifiable lesions. Same region was used for each processing technique, and noise is expressed as the relative root-mean-square deviation of counts from pixel to pixel. Three techniques were compared with each other by paired *t* test.

authors question the need to perform measured attenuation correction on every patient to simply detect malignant lesions (*2*), mainly on the grounds that transmission scanning is a time-consuming process and deteriorates image quality. However, faster transmission and better reconstruction techniques are now available to overcome the limitations of previous methods that used filtered backprojection and nonsegmented coincidence transmissions scans (*11*).

Postinjection transmission scanning allows improvements in patient throughput and delayed imaging by avoiding the need to keep the patient on the scanner bed between the time of injection and acquiring the emission data (*12–15*). Simultaneous emission and transmission scanning has also been proposed as an alternative method to optimize the data acquisition (*16,17*), but these methods are complex to implement and so far have been applied only to two-dimensional acquisition modes. As an alternative to prolonged acquisition times, image segmentation techniques have been proposed to reduce the noise present in short transmission scans (*18*). Transmission scanning with a single-photon emitter, a ^{137}Cs point source, has recently been introduced to perform rapid measured attenuation correction in volume-imaging PET scanners (*4,19*). However, postinjection scans have been demonstrated only with NaI(Tl) systems (*3,20*).

In this study, we evaluated, from a clinical perspective, the relative merits of three processing techniques to provide accurate attenuation correction with ^{137}Cs transmission data. Our results show that segmentation of the transmission data provides final reconstructed images of high quality, with a low noise content, at the expense of some loss of activity gradients in the chest, and therefore a slight underestimation of the activity in some parts of the lungs. The sharp attenuation boundaries introduced by image segmentation may also enhance the edge of the lungs to some extent, but in our experience, this has never been sufficiently intense to be confused with active disease.

ECS is an attractive approach that allows preservation of all density gradients without creating edge artifacts. However, because transmission noise is propagated into the final reconstructed images, these are noisier than those obtained with the other two techniques. Subjectively, the images are more difficult to interpret because of the added noise, and this may reduce diagnostic confidence. THR, a hybrid method that partially segments the EC scan in the soft-tissue density range, preserves the quantitative accuracy and the activity gradients of the ECS method. It is also a more versatile approach than segmentation in complex anatomic areas, such as the head and neck. However, in our current implementation of this algorithm, edge artifacts are not completely eliminated, but again, this rarely, if ever, poses significant diagnostic difficulties.

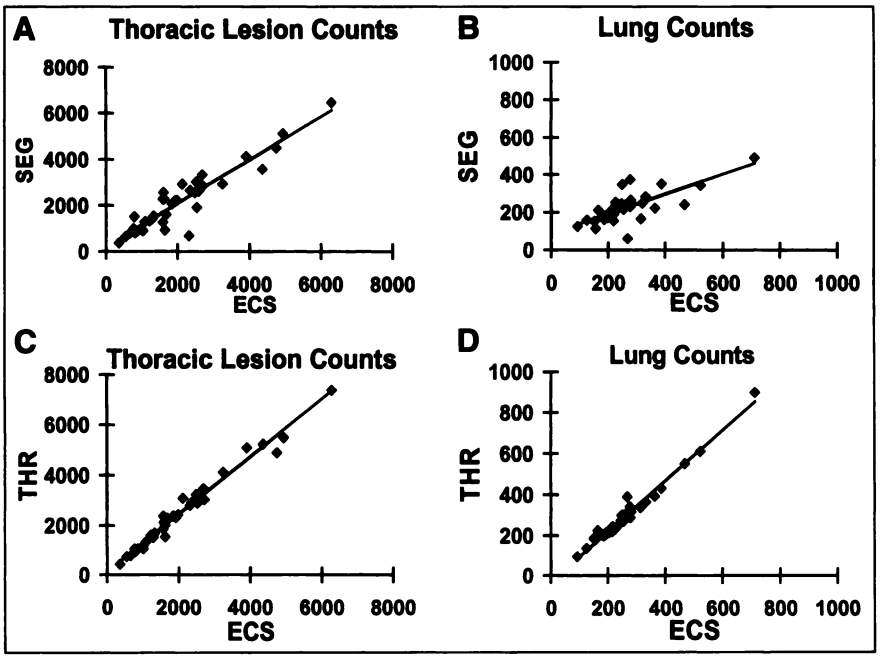

FIGURE 4. Quantitative comparison of count densities from fully corrected scans produced by three techniques. SEG method slightly underestimates activity in chest lesions (A) and lungs (B), whereas there is excellent correspondence between ECS and THR methods (C and D).

Given the choice of three accurate processing methods, choosing one depends on the clinical situation. In general, with the arms outside the FOV, segmentation works well, providing excellent image quality with a low noise content. The other two processing methods perform well in all situations, including complex anatomic areas where more density gradients and more than one body outline can be encountered. These methods also seem to be more accurate to assess the activity in the pulmonary parenchyma and to determine the true activity in small pulmonary nodules that may not be properly segmented as soft tissue by the segmentation algorithm. The importance of these phenomena remains unclear compared with the effects of respiratory motion blurring, but the SEG method has the disadvantage of introducing an additional potential source of error in these situations. Because it introduces noise in the reconstruction of the emission data, the ECS method does not produce images as appealing as those with the THR technique. Recently, however, modifications to the data acquisition electronics have been made for singles transmission scans in the PENN-PET systems. This should lead to increased data collection rates and, thus, improved statistics for the transmission scans without increasing the scan duration. In addition, an energy correction method has been implemented (*7*). By improving the energy resolution, this may allow better discrimination of the emission contamination during the transmission scan. Both of these changes could lead to lower noise in the ECS method.

CONCLUSION

Measured attenuation correction with a rotating ^{137}Cs point source has become a routine procedure for whole-body studies at our PET facility. This enables the acquisition of rapid transmission scans for three-dimensional (septa-less) systems. To take advantage of this technique for fast patient throughput, it is necessary to obtain these scans after injection. Although the uncorrected attenuation coefficients provided by this method are different from the 511-keV values, the three processing methods evaluated here perform well clinically and are applicable for routine use. The quality of the final attenuation-corrected emission images is excellent, as a result of a combination of iterative reconstruction and processing of singles transmission data. Segmentation of the transmission scan remains a simple and effective approach. However, the THR and ECS methods offer additional benefits in preserving the density gradients in the lungs. In particular, THR is an overall attractive approach that combines the best features of the SEG and ECS methods. Refinements in the thresholding and interpolation algorithms could further improve this method by reducing the sharp boundaries that are sometimes observed at the edge of the lung outlines.

ACKNOWLEDGMENTS

Dr. François Bénard was supported by the Medical Research Council of Canada under the clinician-scientist award program. Dr. Joel S. Karp and Robin J. Smith were partially supported by Department of Energy grant DE-FG02–88ER60692 and National Institutes of Health grant NS-14789. We acknowledge the contributions of Drs. Eugene Gualtieri and Gerd Muehllehner, of UGM Medical Systems, Inc., Philadelphia, PA, for implementing and providing the reconstruction software used in this study.

REFERENCES

1. Rigo P, Paulus P, Kaschten B, et al. Oncological applications of positron emission tomography with fluorine-18 fluorodeoxyglucose. *Eur J Nucl Med.* 1996;23:1641–1674.
2. Bengel FM, Ziegler SI, Avril N, Weber W, Laubenbacher C, Schwaiger M. Whole-body positron emission tomography in clinical oncology: comparison between attenuation-corrected and uncorrected images. *Eur J Nucl Med.* 1997;24:1091–1098.
3. Smith R, Karp J, Muehllehner G, Gualtieri E, Bénard F. Singles transmission scans performed post-injection for quantitative whole body PET imaging. *IEEE Trans Nucl Sci.* 1997;44:1329–1335.
4. Karp JS, Muehllehner G, Qu H, Yan XH. Singles transmission in volume-imaging PET with a ^{137}Cs source. *Phys Med Biol.* 1995;40:929–944.
5. Smith R, Karp J, Bénard F, et al. A comparison of segmentation and emission subtraction for singles transmission in PET. *IEEE Trans Nuc Sci.* 1998;45:1212–1218.
6. Chatziioannou A, Dahlbom M, Hoh C. Whole body PET attenuation correction with transmission image segmentation [abstract]. *J Nucl Med.* 1996;37:8P.
7. Smith R, Karp J, Gualtieri E, Muehllehner G. Methods to suppress and correct for scatter and emission contamination of post-injection singles transmission in PET [abstract]. *J Nucl Med.* 1998;39:37P.
8. Karp JS, Muehllehner G. Standards for performance measurements of PET scanners: evaluation with the UGM PENN-PET 240H scanner. *Med Prog Technol.* 1991;17:173–187.
9. Meikle S, Hutton B, Bailey D, Hooper P, Fulham M. Accelerated EM reconstruction in total-body PET: potential for improving tumor detectability. *Phys Med Biol.* 1994;39:1689–1709.
10. Hudson H, Larkin R. Accelerated image reconstruction using ordered subsets of projection data. *IEEE Trans Med Imag.* 1994;1:113–122.
11. Bedigian MP, Bénard F, Smith RJ, Karp JS, Alavi A. Whole-body positron emission tomography for oncology imaging using singles transmission scanning with segmentation and ordered subsets-expectation maximization (OS-EM) reconstruction. *Eur J Nucl Med.* 1998;25:659–661.
12. Turkington T, Coleman R, Schubert S, Ganin A. An evaluation of post-injection transmission measurement in PET. *IEEE Trans Nucl Sci.* 1994;41:1538–1544.
13. Smith R, Karp J. Post-injection transmission scans in a PET camera operating without septa with simultaneous measurement of emission activity contamination. *IEEE Trans Nucl Sci.* 1996;43:2207–2212.
14. Smith R, Karp J, Muehllehner G. Post injection transmission scanning in a volume imaging PET camera. *IEEE Trans Nucl Sci.* 1994;41:1526–1531.
15. Carson R, Daube-Witherspoon M, Green M. A method for postinjection PET transmission measurements with a rotating rod source. *J Nucl Med.* 1988;29:1558–1567.
16. Thompson C, Ranger N, Evans A. Simultaneous transmission and emission scans in positron emission tomography. *IEEE Trans Nucl Sci.* 1989;36:1011–1016.
17. Meikle SR, Bailey DL, Hooper PK, et al. Simultaneous emission and transmission measurements for attenuation correction in whole-body PET. *J Nucl Med.* 1995;36:1680–1688.
18. Xu M, Luk W, Cutler PD, Digig WM. Local threshold for segmented attenuation correction of PET imaging of the thorax. *IEEE Trans Nucl Sci.* 1994;41:1532–1537.
19. de Kemp R, Nahmias C. Attenuation correction in PET using single photon transmission measurements. *Med Phys.* 1994;21:771–778.
20. Shao L, Nellemann P, Muehllehner G, Bertelsen H, Hines H. Singles-transmission attenuation correction for dual-head coincidence imaging [abstract]. *J Nucl Med.* 1998;39:37P.